Eur Biophys J (1996) 24: 335–341

ARTICLE

Manuel Cortijo · Carmen Santisteban
Beatriz Carrero-González · Jesus Alvarado
Jesus Ruiz-Cabello

Improvement of functional magnetic resonance images by pretreatment of data

Received: 24 October 1995 / Accepted: 13 February 1996

Abstract Functional magnetic resonance images of the brains of subjects performing the finger-tapping paradigm were made using a conventional technique. Two threshold values for the pixels were obtained by analysing pixel by pixel the distributions of the means and variances of each subject's images for 20 consecutive scans, both while performing the task and while at rest. Considerable signal improvement in the final images was achieved by removing from our data all pixels beyond these threshold values (mean ≤ 16 and variance ≥ 7).

Key words fMRI · Finger-tapping paradigm

Introduction

Functional magnetic resonance imaging (fMRI) has become a powerful tool in the detection and assessment of cerebral pathophysiology and the regional mapping and characterization of such cognitive processes as vision, motor skills, language and memory (Sanders and Orrison 1995; Kucharczyk et al. 1995). Neural activity is associated with local changes in cerebral blood flow, blood volume and oxygenation (Paulson and Sharbrough 1974; Fox et al. 1986; 1988; Belliveau et al. 1991). Pioneer fMRI studies showed changes in regional cerebral blood flow in response to sensory stimulation by using an ultrafast NMR imaging technique and a paramagnetic contrast agent (Belliveau et al. 1990; 1991). More and more, non-contrast-based NMR methods are being used as a non-invasive alternative to other functional imaging techniques (see Sanders and Orrison 1995; Kucharczyk et al. 1995 and references therein), such as positron emission tomography (PET) and single photon emission computerized tomography (SPECT).

The physiological basis for brain mapping by non-invasive fMRI is presumed to lie mainly with a transient hyperoxygenation of the venous blood pool associated with neural activity, caused by an increase in oxygen demand and consequently a regional increase in cerebral blood flow (the blood oxygen-level-dependent, BOLD effect). Signal alterations in certain brain regions have also been suggested to be related to large vessels (vascular noise), and with flow changes which increase the MRI signal by reducing spin saturation (the in-flow effect) (Duyn et al. 1994). Since some of these mechanisms are associated with the NMR parameters used in the acquisition of data, the interpretation of activation maps in fMRI will require detailed information concerning the experimental conditions under which the images were made and the methods used in their reconstruction (Frahm et al. 1993; Ogawa et al. 1995).

Using fMRI, an image is essentially obtained by making a pixel by pixel comparison of image sequences corresponding to periods while the subject is performing a given task (activation image) and while he/she is not (at-rest image). The very low signal changes ($\Delta S/S$) associated with these experiments [about 8% at 1.5 T (Ogawa et al. 1993; 1995; Turner et al. 1991)] are within the range in which a number of potential artefactual sources, such as the bulk motion of the subject during the experiment, pulsatile blood, or other such non-stimulus processes, may contribute. For example, tiny spatial misalignment between scans may cause artefactual signal differences at the boundaries between two images of as much as 40% (Turner 1994).

Pulse sequences less sensitive to these intrusions must therefore be used and powerful statistical methods need to be applied to the data processing (see Sanders and Orrison 1995; Poline et al. 1995; Kucharczyk et al. 1995 and references therein). Less powerful methods, such as the single subtraction of pixel data between activation and at-rest

M. Cortijo (✉) · B. Carrero-González · J. Ruiz-Cabello
Departamento de Química Física II, Facultad de Farmacia,
Unidad de RMN, Instituto Pluridisciplinar,
Universidad Complutence, E-28040 Madrid, Spain

C. Santisteban · J. Alvarado
Departamento de Metodologia, Facultad de Psicología,
Unidad de RMN, Instituto Pluridisciplinar,
Universidad Complutence, E-28223 Madrid, Spain

images for example, are very susceptible to noise, particularly where small changes in large signals are concerned. Thus, to demonstrate more clearly the potential of the pre-processing approach we describe here, we have generally used the single subtraction of pixels. For the same reason, we have used a conventional MRI scanner without specialised hardware for fast imaging sampling and also a conventional gradient-echo sequence. With echo-planar technology, specialised hardware and better data processing the great advantages of the pre-processing technique discussed in this paper would not be so evident.

We obtained repetitive fast images, both activation and at-rest, which allow us to obtain the frequency distributions of the means and variances of the pixels. By studying these distributions we were able to choose threshold values for both the means and variances of the pixels in the resting images, which improve the quality and reliability of the fMR images considerably.

Methods

1. NMR data acquisition and processing

The scans were made on a 1.5-tesla scanner (GE Medical Systems Signa, Milwaukee, WI) using a standard quadrature head coil. Sagittal multisection T 1-weighted images were obtained as an anatomical guide to select the correct planes for activity studies. For a motor stimulation, an axial plane through the primary motor and sensory cortex was chosen. T 1-weighted images were obtained and used as anatomical references for the brain-activity maps. For the motor-activity studies, these identical selected planes were then imaged by using a conventional gradient-echo acquisition (TR = 120 ms, TE = 45 ms, flip angle = 40°, NEX = 2, flow compensation, FOV = 22 cm, slice thickness = 10 mm, imaging matrix = 128×256) with a scan time of 30 s. The task for each time course series was divided into two consecutive periods, and a sequence of ten gradient-echo images was taken within each of these. The subjects were asked beforehand to remain completely relaxed during the first period (at-rest images), and during the second one to perform the finger-tapping paradigm by touching each right-hand finger to the thumb in a sequential, self-paced, repetitive manner (activation images). All the images displayed were linearly interpolated to a 256×256 matrix. Twelve right-handed subjects between 19 and 25 years of age, all members of the university, participated in the experiments. Their written informed consent was obtained beforehand.

All processing was performed off-line with home-developed software in UNIX based workstations by using Interactive Data Language (Research Systems, Boulder, Colorado). Threshold images of the cerebral-activity images were obtained from the time course data as described above, and superimposed upon the spin-echo anatomical references.

2. Statistical methods

The images corresponding to both resting and activity periods were represented by matrices of mxm = M dimensions, where M is the total number of pixels (mxm = 256×256 in our case). The values for each i, j pixel in the k scan are x_{ijk} and y_{ijk} under the resting and activity conditions respectively ($i = 1, 2, \ldots, 256$; $j = 1, 2, \ldots, 256$ and $k = 1, 2, \ldots, 10$). For every ten-images sequence, acquired for both the resting and activity periods, the corresponding means: $\bar{x}_{ij} = (\sum_k x_{ijk})/10$ and $\bar{y}_{ij} = (\sum_k y_{ijk})/10$ and variances:

$$\sigma_x^2 = \sigma^2(x_{ij}) = \sum_k (x_{ijk} - \bar{x}_{ij})^2/10; \sigma_y^2 = \sigma^2(y_{ij}) = \sum_k (y_{ijk} - \bar{y}_{ij})^2/10$$

were calculated for each i, j pixel. From now on we only use these four matrixes ($\bar{x}_{ij}$, $\bar{y}_{ij}$, σ_x^2 and σ_y^2) for each subject.

Two methods, means subtraction and Student's t test, were used for image comparison between the resting and task-performing periods. In a forthcoming publication, we shall be comparing the results obtained when using other parametric and non parametric methods.

The distributions of variances ($z = \sigma_x^2$) are fitted to the beta distribution in order to determine the value and significance of the variances threshold (Johnson et al. 1995). The continuous beta distribution, Be (v_1, v_2), is defined by the following probability density function (Wilks 1962)

$$f(z) = \frac{\Gamma(v_1 + v_2)}{\Gamma(v_1)\,\Gamma(v_2)} z^{v_1 - 1}(1 - z)^{v_2 - 1}$$

for $0 < z < 1$ and $f(z) = 0$ elsewhere. We have used the moments method (Kendall and Stuart 1963, 1967) for the fitting procedure, where the first, $\hat{\alpha}_1$, and second, $\hat{\alpha}_2$, moments are $\hat{\alpha}_1 = \sum z/n$; $\hat{\alpha}_2 = \sum z^2/n$, being $v_2 = (\hat{\alpha}_2 \hat{\alpha}_1 - \hat{\alpha}_2 + \hat{\alpha}_1 - \hat{\alpha}_1^2)/(\hat{\alpha}_2 - \hat{\alpha}_1^2)$ and $v_1 = (\hat{\alpha}_2 v_2 + \hat{\alpha}_2 - \hat{\alpha}_1)/(\hat{\alpha}_1 - \hat{\alpha}_2)$ and n is the total number of pixels considered.

Results

The $\bar{x}_{ij}$ and $\bar{y}_{ij}$ values obtained in our studies ranged from 0 to 200 in arbitrary units. One of the fMR images obtained by plotting only $\bar{y}_{ij} - \bar{x}_{ij}$ differences of pixels greater than 2 arbitrary units is shown in Fig. 1 A. It contains a lot of artefactual noise because, as its presence is intentional, we have used a low threshold value and have taken no experimental step to avoid it (cf. Introduction). The situation can be improved a lot by using a more powerful statistical technique such as the Student's t test (Fig. 1 B), although there are still many false positives (e. g. signal differences remaining outside the brain area).

The frequency distribution of the $\bar{x}_{ij}$ values for each i, j and one subject's image is plotted in Fig. 2 A. We obtained very similar results with the other subjects. The distributions always showed a first population with a maximum at $\bar{x}_{ij}$ of about 3 and another with a smaller maximum of about 90. Practically identical distributions are ob-

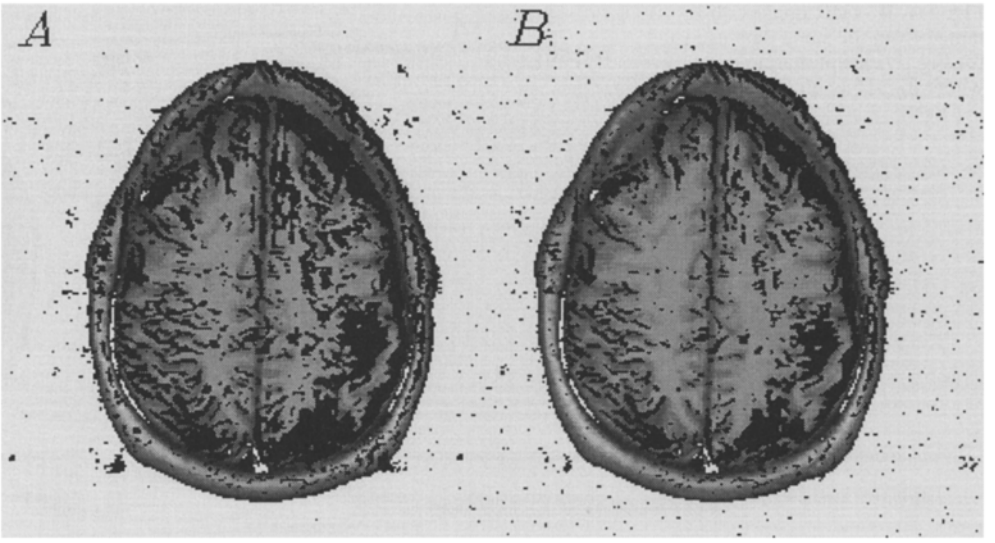

Fig. 1 A, B fMR images obtained for one subject performing the finger-tapping paradigm under the experimental conditions described in the text and superimposed upon the corresponding spin-echo anatomical images. **A** Only those pixels showing $\bar{y}_{ij}-\bar{x}_{ij}$ values greater than 2 arbitrary units are plotted. **B** Student's t test ($\alpha=0.01$) for the same data

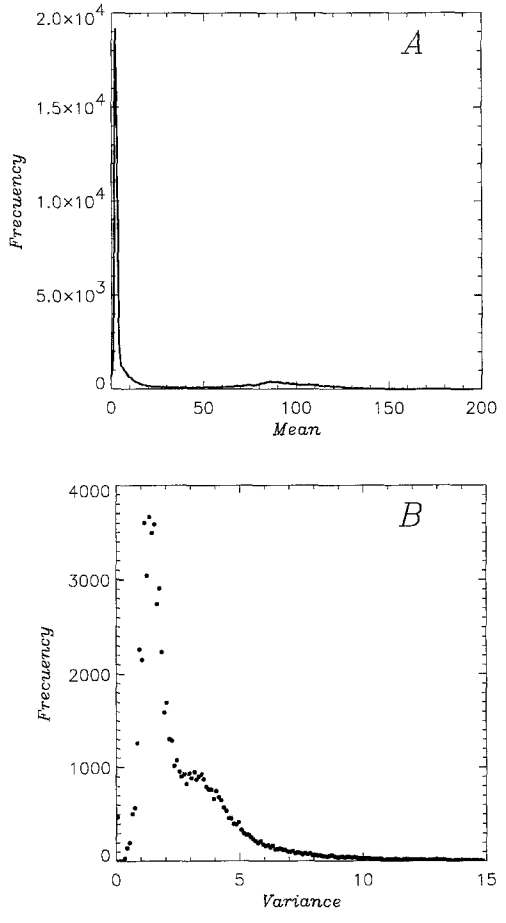

Fig. 2 A, B Frequency (number of pixels) of $\bar{x}_{ij}$ (**A**) and σ_x^2 (**B**) for the data used for Fig. 1

tained when the $\bar{y}_{ij}$ frequencies are plotted (results not shown), owing to the very small differences between $\bar{y}_{ij}$ and $\bar{x}_{ij}$ in fMRI. The frequency distribution of σ_x^2 values is given in Fig. 2 B, which also shows two populations of pixels. Similar results are obtained for the frequency distribution of variances for the activation images (results not shown). It is worthy of remark that we have always obtained two populations (neither one nor more than two) for both means and variances frequency plots. The first pixel population (those where $\bar{x}_{ij} \leq 16$) will lead to very small signal changes ($\Delta S \approx 1$), because $\Delta S/S$ lower than 8% must be expected at 1.5 T (cf. Introduction). Therefore, the $\bar{y}_{ij}-\bar{x}_{ij}$ differences for these pixels will always be confused with the experimental noise (including data digitalization) and we think is worthwhile considering all the $\bar{y}_{ij}-\bar{x}_{ij}$ differences obtained for this first data population (where $\bar{x}_{ij} \leq 16$) as being artefactual errors. Thus we decided to remove all pixels where $\bar{x}_{ij} \leq 16$ from our data. The fMR images now obtained are depicted in Fig. 3 A and B, which show a great improvement compared with Fig. 1 A and B. By this comparison we can see that the pixels removed from Fig. 1 are randomly distributed along the brain. This observation shows that the two data populations do not correspond to two different brain regions (for example, grey and white matter) and fortifies our assumption that the first one (that with values of $\bar{x}_{ij} < 16$) is only due to artefactual errors. There are nevertheless still some false positives in Fig. 3, which prevent us seeing the expected activation areas clearly.

The frequency distributions of means ($\bar{x}_{ij}$) and variances (σ_x^2) for pixels where $\bar{x}_{ij} > 16$ are shown in Fig. 4 A and B, respectivley. We can now see one maximum in the means frequency plot, at about $\bar{x}_{ij} = 90$ and a shoulder at about $\bar{x}_{ij} = 110$ (Fig. 4 A). These two populations appear with all twelve subjects studied, although their relative positions, height and overlap alter from one individual to another (results not shown). The variances frequency plots (Fig. 4 B) always showed a single maximum of about $\sigma_x^2 = 3.5$. We do not see now the first population of pixels with a maximum about $\sigma_x^2 = 1.3$ shown in Fig. 2 B. This means that it corresponds exclusively to the first media population with maximum at $\bar{x}_{ij} = 3$. Therefore, our data unambiguously indicate that, within our experimental resolution, different brain regions can be fitted by a single variances distribution.

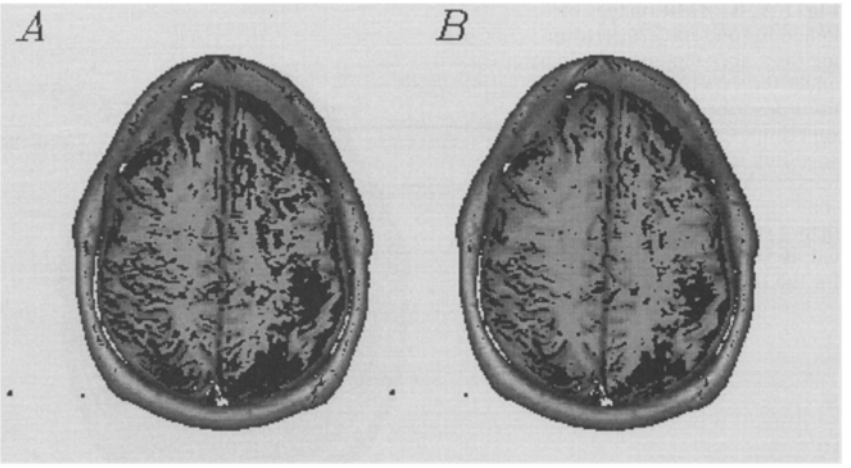

Fig. 3 A, B fMR images obtained from the same data used for Fig. 1, except that no data where $\bar{x}_{ij} \leq 16$ is plotted

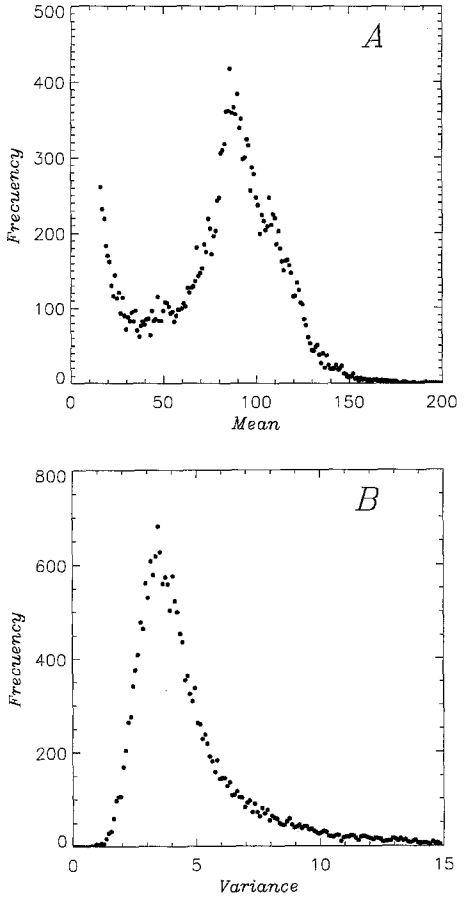

Fig. 4 A, B Frequency distribution of $\bar{x}_{ij}$ (**A**) and σ_x^2 (**B**) for the data used for Fig. 3

These variances came from measurements of the variations obtained in k repeated measures taken in the same pixel, under identical experimental conditions, with the same subject and during a short time interval. We must then expect low variances, due to random variations, and it appears to us that a good filter could be obtained by removing all data with larger variances than a given threshold value. To find this value it is convenient to fit the variances population to a given distribution function. We have not fitted our data to a chi-squared distribution, despite the fact that we are dealing with sums of squares variables, because these variables should be normally distributed and independent, and we are not sure that any of these conditions is fulfilled here. Therefore, we have employed a beta distribution, with parameters $\nu_1 \ll \nu_2$, which is empirically used in a wide range of applications (Johnson et al. 1995). The values of ν_1 and ν_2 found are very similar for all subjects (around $\nu_1 = 2$, and $\nu_2 = 16$). The probability of having pixels with variances lower than twice the distribution mode is always about 85% in both the experimental and the theoretical distributions. We therefore tried to improve our results by removing those data with variances greater than this threshold value ($7 = 2 \times 3.5$). This improvement is clearly shown in Fig. 5 A and B, where only pixels with values of $\bar{x}_{ij} > 16$ and $\sigma_x^2 < 7$ are plotted. Although artefacts may still be present, the expected activation area (marked with an arrow) can now be clearly seen as the larger cluster of points (see the differences between these and the similar Fig. 3 A and B). The great improvement resulting from using a parametric statistical technique such as Student's t test (Fig. 5 B) compared to the results obtained by using a simple subtraction method (Fig. 5 A) also becomes evident. Further comparison with other parametric and non-parametric methods will be done in a forthcoming article.

The central issue in fMRI studies is how the observed activation image relates to the *real* site of neural activity. We know the location of the site which is activated while right-handed subjects perform the finger-tapping paradigm by reference to previous studies reported in the literature, either using fMRI (Connelly et al. 1993; Bandettini et al. 1994; Kim et al. 1994) or other techniques (cf. Fig. 7.101 in Sanders and Orrison 1995). Small changes can be expected in a small area along the gyral surface of the anterior margin of the central sulcus of their left hemisphere, minimal activation in areas anterior to this (premotor regions), and essentially no activation along the central sulcus of the right hemisphere (Latchaw et al. 1995). This means that we should on the whole expect activation in-

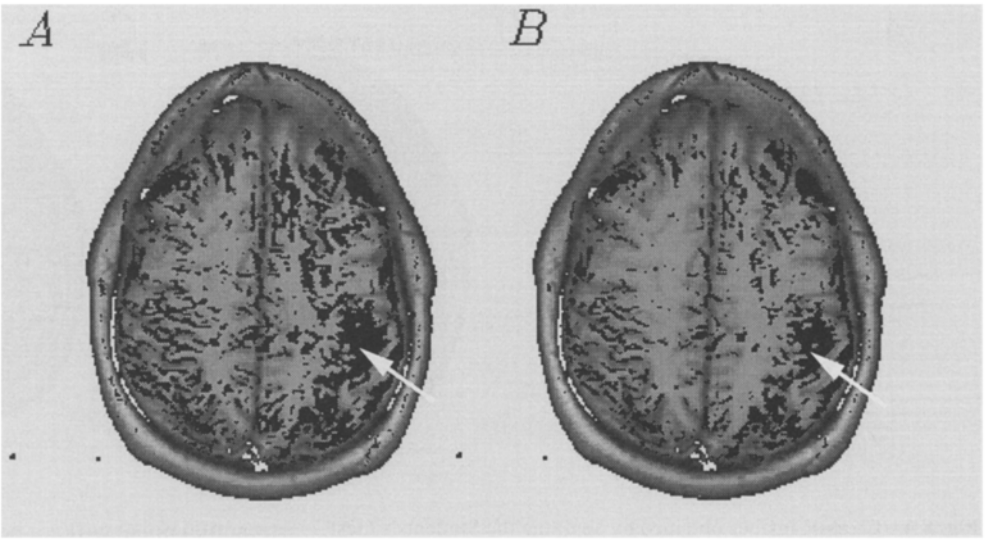

Fig. 5 A, B fMR images obtained for the same data used for Fig. 1 except that no data where $\bar{x}_{ij} \leq 16$ and $\sigma_x^2 \geq 7$ is plotted

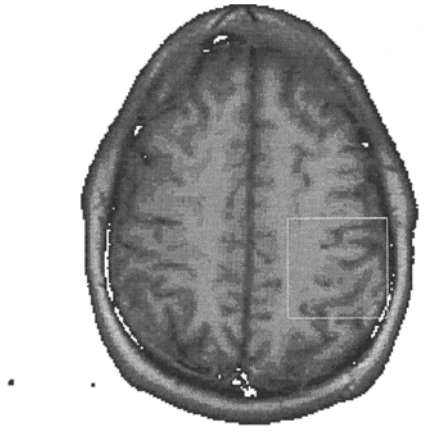

Fig. 6 Region of interest (ROI) in our studies

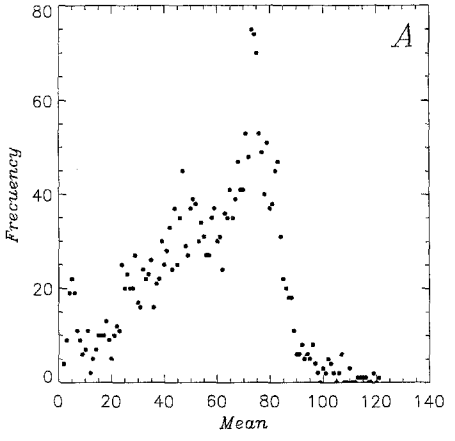

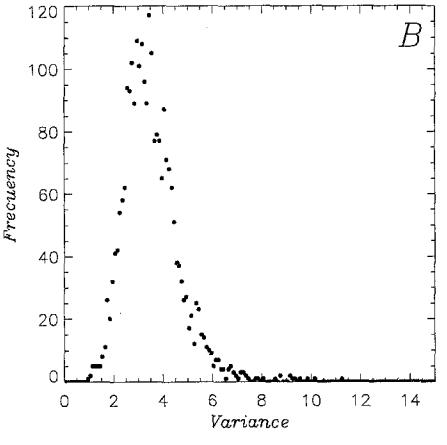

Fig. 7 A, B Frequency distribution of $\bar{x}_{ij}$ (**A**) and σ_x^2 (**B**) for those pixels inside the ROI selected in Fig. 6

side the region of interest (ROI) shown in Fig. 6. When we study the frequency distributions for all pixels inside this ROI we see that there is little data for $\bar{x}_{ij} \leq 16$ and $\sigma_x^2 \geq 7$, thus supporting our choice of these threshold values (Fig. 7). The presence of only a few pixels in the ROI beyond these threshold values was observed with all twelve subjects (results not shown), irrespective of the position and size of the ROI (only reasonable values were tested). Some claims have been made that results obtained by using selected ROIs are highly dependent upon the location and size of the ROI (Sanders and Orrison 1995). We do not need to involve ourselves in this point here because the virtual absence of pixels in our selected ROIs beyond the two threshold values ($\bar{x}_{ij} = 16$ and $\sigma_x^2 = 7$) means that by using our removal procedure we are not increasing type II errors (i. e. the probability of overlooking true changes), at least with fMR images of subjects performing the finger-tapping paradigm.

It may reasonably be inferred from these results that a significant signal improvement should be obtained by eliminating from the data matrices those pixels which in the resting state have a very low signal value ($\bar{x}_{ij} \leq 16$) and the remainder with variances equal to and greater than 7. Further improvements in the quality of the fMR images must depend mainly upon the use of better experimental conditions (purpose-designed coils, ultra-fast echo-planar sequences and so on), and the use of better statistical meth-

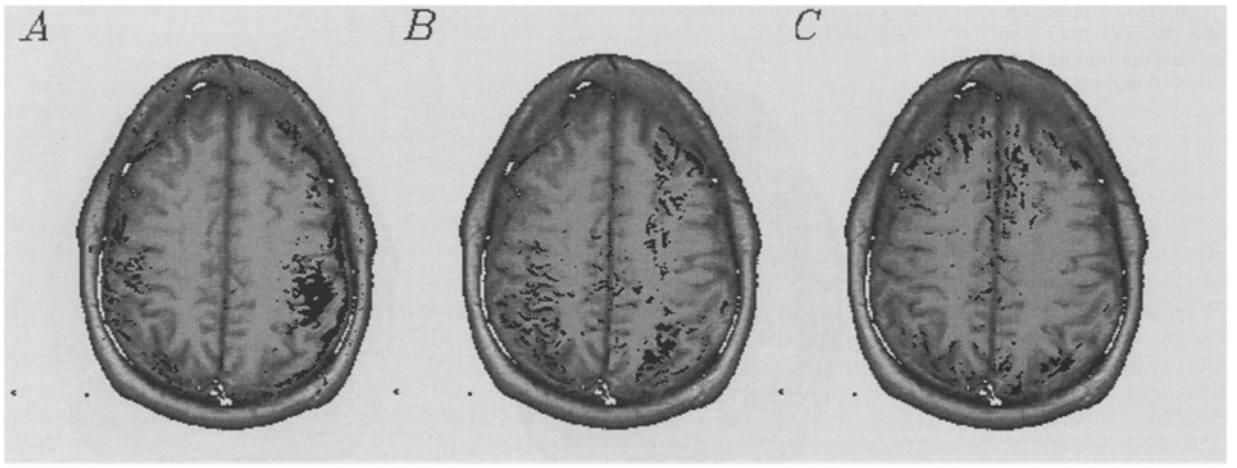

Fig. 8 A – C fMR images obtained by applying the Students's *t* test (α=0.01) of those pixels where $\sigma_x^2 < 7$ and **A**: $16 < \bar{x}_{ij} \leq 68$; **B**: $68 < \bar{x}_{ij} \leq 90$ and **C**: $90 < \bar{x}_{ij}$

ods that decrease type I errors (i. e. the probability of detecting false positives), despite the fact that this may bring about an increase in type II errors.

Discussion

fMRI has proved to be a promising and powerful tool for non-invasive, incruent studies into cerebral pathophysiology and the mapping of cognitive processes in the brain. One of the main problems pertaining to this technique, which impeded its wider development, is the difficulty in correlating the activity observed and the *real* sites of neural activity, owing to the very low signal-to-noise ratios involved in these experiments. To overcome this, many technical advances and very powerful statistical methods have been applied to decrease artefactual noise and increase the significance of the results. The problem revolves essentially around maximizing the probability of detecting true changes (i. e. decreasing type II errors) and simultaneously minimizing the probability of detecting artefactual signals (i. e. decreasing type I errors).

We chose a conventional gradient-echo sequence for our data acquisition, this technique being very sensitive to small motions. When we compare our Figs. 1 A and 3 A or Figs. 1 B and 3 B we see that a great deal of boundary noise disappears as a simple result of removing those pixels where $\bar{x}_{ij} \leq 16$. We are aware that some noise is still present after this filtering process but this implies that our method will also improve the reliability of measurements performed with sequences less sensitive to noise than the one used here, such as, for example, gradient-echo planar techniques. Moreover, when Figs. 1 and 5 are compared we see that more false-positives disappear in the frontal area than in back brain positions. More motion noise might be expected in the frontal area, due to involuntary movements when the subjects start the task. This could well imply that artefactual noise will not be uniformly distributed in fMRI, even when using better technology. However, when algorithms (Hajnal et al. 1995; Baudendistel et al. 1995) for correction of slight head movements are used for image matching we did not see appreciable differences with respect to the images without such correction for our twelve subjects, although some mismatchings were detected and corrected in several cases.

The threshold value of 15% of probability in the beta distributions (or twice the mode) for discarding pixels with large variances is of course arbitrary and it depends on our subjective demanding level. It is convenient to say, however, that fMR images are almost equal by using threshold values between 10 and 20%. These computations clearly need to be recalculated every time the experimental design or the acquisition system is changed. However the computation is easily made and takes little additional time, because the means must always be calculated independently of the statistical method used. It is worth noting that t-maps, as well as other statistical methods, are discarding data based on the ratio between means differences and error variances and then data with high error variances cannot be excluded in the maps if the means differences are high enough. Therefore, we think that is advisable to discard these data with large error variances in a pre-treatment process. Furthermore, the overlapping between the $\bar{x}_{ij}$ and $\bar{y}_{ij}$ distributions increases with the error variances, raising the β-error and so lowering the power of the test (1-β). This means that we are lowering the type II errors by eliminating pixels with large error variances during the data pretreatment.

We have clearly shown here that a preliminary filtering of data, carried out by eliminating those pixels in the resting state that show $\bar{x}_{ij} \leq 16$ and a subsequent removal of those remaining showing $\sigma_x^2 \geq 7$, could be an easy and highly desirable step for starting data manipulation in any fMRI experiment. These numbers (16 and 7) can also be optimized for each particular case without too much effort and many time-consuming computations by following a similar process to that described here.

The study of frequency means distributions in the whole brain (Fig. 4 A) and in the ROI (Fig. 7 A) can also help to

improve the quality of the final fMR images. From our distributions we can estimate three pixel populations with the limits given in the caption of Fig. 8, which is obtained by plotting the $\bar{y}_{ij} - \bar{x}_{ij}$ differences of those pixels were $\sigma_x^2 < 7$ and $\bar{x}_{ij}$ is within the indicated limits. The last population (C) has not pixel in our selected ROI (cf. Fig. 7 A). Fig. 8 A is surprisingly similar to what we might expect to obtain under more precise experimental conditions. The pictures are not very sensitive to small changes in the limits, which alter slightly from one subject to another, and the final images are always very similar (results not shown). These limit changes were not made on subjective grounds; for example, we included a line in our computer program to detect them when the first derivate of the curve given in Fig. 4 A reached values of −1 and +1. Any other objective criterion may be used. We are aware that Fig. 8 A still contains artefactual signals. Neither did we instruct our subjects to avoid other tasks while they were performing the finger-tapping paradigm. For example, we found out afterwards that some of them were following the paradigm with their eyes whilst others where simultaneously enacting the silent word-generation paradigm, and some contamination from these tasks must then be expected in our data. We should like to point out, however, that disentangling the images by a careful study of the frequency means distribution functions, as has been done in Fig. 8, simplifies the results and helps to identify more elaborate physiological consequences, which we do not try to do here for the reasons mentioned above. We intend to do this in a forthcoming article in which we operate under better experimental conditions and apply and compare more powerful statistical techniques.

Acknowledgements This work was supported by grants PB91-0368 and PB92-0207 from DGICYT, Spain. B. C. G. acknowledges a fellowship from CAM, Spain. We thank Dr. Felipe Esteban-Alonso for all the facilities he provided to make our measurements with the NMR instrument at the "Hospital del Aire", UCM, Madrid and Mrs. Marien Fernández for her computer assistance. We also thank Dr. J. Trout for revising the English text.

References

Bandettini PA, Wong EC, Jesmanowicz A, Hinks RS, Hyde JS (1994) Spin-echo and gradient-echo EPI of human brain activation using BOLD contrast: a comparative study at 1.5 T. NMR Biomed 7: 12–20

Baudendistel K, Schad LR, Friedlinger M, Wenz F, Schröder J, Lorenz WJ (1995) Postprocessing of functional MRI data of motor cortex stimulation measured with s Standard 1.5 T Imager. Magn Reson Imaging 13: 701–707

Belliveau JW, Rosen BR, Kantor HL, Rzedzian RR, Kennedy DN, McKinstry RC, Vevea JM, Cohen MS, Pykett IL, Brady TJ (1990) Functional cerebral imaging by susceptibility-contrast NMR. Mag Reson Med 14: 538–546

Belliveau JW, Kennedy DN, McKinstry RC, Buchbinder BN, Weisskoff RM, Cohen MS, Vevea JM, Brady TJ, Rosen BR (1991) Functional mapping of the human visual cortex by magnetic resonance imaging. Science 254: 716–719

Connelly A, Jackson GD, Frackowiak RSJ, Belliveau JW, Vargha-Khadem F, Gadian DG (1993) Functional mapping of activated human primary cortex with a clinical MR imaging system. Radiology 188: 125–130

Duyn JM, Moonen CTN, van Ypereu GH, de Boer RW, Luyten PR (1994) Inflow versus deoxyhemoglobin effects in BOLD functional MRI using gradient echoes at 1.5 T. NMR Biomed 7: 83–88

Fox PT, Mintun MA, Raichle ME, Wiezin FW, Allman JM, Van Essen DC (1986) Mapping the human visual cortex with positron emission tomography. Nature 323: 806–809

Fox PT, Raichle ME, Mintun MA, Dence C (1988) Nonoxidative glucose consumption during focal physiologic neural activity. Science 241: 462–464

Frahm J, Merboldt KD, Hänicke W, Kleinschmidt A, Boecker M (1993) Brain or vein-oxygenation or flow? On signal physiology in functional MRI of human brain activation. NMR Biomed 7: 45–53

Hajnal JV, Saeed N, Soar EJ, Oatridge A, Young IR, Bydder GM (1995) A registration and interpolation procedure for subvoxel matching of serially acquired MR images. J Comput Assist Tomogr 19: 289–296

Johnson ML, Kotz S, Balkirshan N (1995) Continuous univariate distributions, 2nd end. Wiley, New York, pp 210–275

Kendall MG, Stuart A (1963) The advanced theory of statistics. Distribution theory, 2nd edn. Griffin, London

Kendall MG, Stuart A (1967) The advanced theory of statistics. Inference and relationship, 2nd edn. Griffin, London

Kim S, Hendrich K, Hu X, Mortle H, Ugurbil K (1994) Potential pitfalls of functional MRI using conventional gradient-recalled echo techniques. NMR Biomed 7: 68–74

Kucharczyk J, Moseley ME, Roberts T, Orrison WW (1995) Neuroimaging clinics of North America (Volume 5: Functional neuroimaging). Saunders, Philadelphia

Latchaw RE, Ugurbil K, Hu X (1995) Functional MR imaging of perceptual and cognitive functions. Neuroimaging Clinics North Am 5: 193–205

Ogawa S, Lee TM, Barrere B (1993) The sensitivity of magnetic resonance image signals of a rat brain to changes in the cerebral venous blood oxygenation. Magn Reson Med 29: 205–210

Ogawa S, Menon R, Ugurbil K (1995) Current topics on the mechanism of fNMRI signal changes. Quart Magn Res in Biol Med 2: 43–49

Paulson OB, Sharbrough FW (1974) Physiologic and pathophysiologic relationship between the electroencephalogram and the regional cerebral blood flow. Acta Neurol Chicago 50: 194–220

Poline JB, Worsley KJ, Holmes AP, Frackowiak RSJ, Friston KJ (1955) Estimating smoothness in statistical parametric maps: variability of p values. J Comput Assist Tomogr 19: 788–796

Sanders JA, Orrison WW (1995) Functional magnetic resonance imaging. In: Orrison WW, Lewine JD, Sanders JA, Hartshorne MF (eds) Functional brain imaging. Mosby, New York, pp 239–326

Turner R, LeBihan D, Moonen CTW, Despres D, Frank J (1991) Echo-planar time course MRI of cat brain oxygenation changes. Magn Reson Med 22: 159–166

Turner R (1994) Magnetic resonance imaging of brain function. Ann Neurol 35: 637–638

Wilks SS (1962) Mathematical statistics. Wiley, London